Journal of Organometallic Chemistry 743 (2013) 1–9

Contents lists available at SciVerse ScienceDirect

Journal of Organometallic Chemistry

journal homepage: www.elsevier.com/locate/jorganchem

Study on the structure–property relationship in a series of novel BF_2 chelates with multicolor fluorescence

Qi-Chao Yao, Ding-Er Wu, Ru-Zheng Ma, Min Xia*

Department of Chemistry, Zhejiang Sci-Tech University, Hangzhou 310018, PR China

ARTICLE INFO

Article history:
Received 17 March 2013
Received in revised form
5 June 2013
Accepted 11 June 2013

Keywords:
Multicolor fluorescence
N,*O*-bidentate BF_2 complex
Structure–property correlation
Photophysical performance
Electrochemical behavior
DFT calculation

ABSTRACT

A series of multicolor fluorescent *N*,*O*-bidentate BF_2 complexes with variable ligand structures have been synthesized. These complexes exhibit the solvent-independent optical properties and large Stoke shifts. The electrochemical measurements demonstrate that all these chelates are better electron acceptors than the commonly used material Alq_3. A qualitative structure–property relationship among these complexes has been established on the ground of the experimental data along with the density functional theory (DFT) calculations. The theoretically calculated results are in good agreement with those obtained by the experimental determinations.

1. Introduction

Organoboron complexes are one of the most important types of fluorescent dyes. Among them, boron dipyrromethenes (BODIPYs) are the most well-known fluorophores with *N*,*N*-bidentate ligands [1–3]. Due to the outstanding properties such as high fluorescence quantum yields and extinction coefficients, excellent photochemical- and chemical-stability, long excited-state lifetimes, large two-photon cross-sections for multiphoton excitation, good solubility, and narrow emission spectra with high color purity, this type of complexes are widely used as chemosensors [4–10], laser dyes [11,12], sensitizers in solar cells [13,14], probes in detecting molecular rotor viscosity [15,16] as well as agents in photodynamic therapy [17,18]. Apart from BODIPYs, other fluorescent organoboron complexes with novel *N*,*N*-bidentate ligands such as pyridomethenes [19,20], pyridylimidazoles [21–23] and others [24–30] have been continuously developed.

However, compared with *N*,*N*-bidentate organoboron fluorophores, the research on their cousins, *N*,*O*-bidentate complexes, is relatively limited. Actually, *N*,*O*-bidentate compounds contain the properties which are different from those of BODIPYs. For example, the Stokes shifts of the typical BODIPYs are very small (usually less than 30 nm) due to their rigid structures. Such small shifts usually result in the serious self-absorption of fluorescence and the decreased quantum yields. Contrarily, the shifts of *N*,*O*-bidentate complexes are so much large (more than 40 nm [31–33]) that discrimination against the incident and the emitted rays, which is very crucial for fluorescent bioanalysis, can be dramatically improved. Additionally, typical BODIPYs are faint or non-fluorescent in solid state owning to the strong π–π stacking of the planar fluorophores, so that excitation energy through the electronic interactions among molecules is substantially dissipated. Such drawback can be efficiently overcome in cases of *N*,*O*-bidentate organoboron complexes. Many of them turn to be intensely fluorescent in aggregated or solid state [34,35]. This property enables them to be as the appealing materials in field of organic electroluminescence devices (OLEDs). Interestingly, a few of *N*,*O*-bidentate organoboron complexes exhibit the attractive aggregation-induced emission (AIE) effect [36]. These complexes with the AIE effect can be exploited as indicators for viscosity and vapor pressure. Therefore, it is quite necessary to develop more and more novel *N*,*O*-bidentate organoboron complexes and explore their intriguing properties.

Although we have carried out some primary research on the BF_2 complexes with 2-(arylethylidene)-3,4-dihydroquinoxalin-2(1H)-one ligands [37], it is still significant to reveal the structure–property relationship for this type of BF_2 chelates based on the detailed measurements and the theoretic calculations. Herein we

---

* Corresponding author. Tel.: +86 571 86843757.
E-mail address: xiamin@zstu.edu.cn (M. Xia).

http://dx.doi.org/10.1016/j.jorganchem.2013.06.012

describe the synthesis, characterization, determination of the optical and electrochemical properties along with the DFT calculations of these multicolor-emitting BF_2 chelates.

2. Experimental

2.1. Materials and measurements

All the reagents used were analytically pure and some chemicals were further purified by recrystallization or distillation. Melting points were determined by an OptiMelt automated melting point system. The ^{1}H NMR (400 MHz), ^{13}C NMR (100 MHz), ^{11}B NMR (128 MHz) and ^{19}F NMR (376 MHz) spectra were obtained on a Bruker Avance II DMX400 spectrometer using DMSO-d_6 or $CDCl_3$ as the solvent. The ^{1}H and the ^{13}C NMR experiments were carried out using tetramethylsilane as the internal standard while the ^{11}B and the ^{19}F NMR spectra were recorded using BF_3OEt_2 (0 ppm) and CF_3COOH (76.5 ppm) as the external standards, respectively. The absorption spectra were measured on a Shimadzu UV 2501(PC)S UV–vis spectrometer and the fluorescence spectra were acquired on a Perkin–Elmer LS55 spectrophotometer. The quantum yields were measured with quinine sulfate in 0.1 M sulfuric acid ($\Phi_f = 0.55$) or fluorescein in 0.1 N NaOH ($\Phi_f = 0.91$) as the reference. The cyclic voltammograms were obtained on a ChenHua CHI660b electrochemical working station with 2 mM sample in anhydrous acetonitrile solution of 0.1 M tetrabutylammonium perchlorate, using a carbon glass as the working electrode, a platinum wire as the counting electrode and a Ag/$AgNO_3$ (0.01 M) pair as the reference electrode. The scan rate was at 30 mV/s with 0.5 mM ferrocene (Fc/Fc^+) as the internal standard. The absolute HOMO energy level of Fc/Fc^+ is assumed as −4.88 eV [38]. The $E_{1/2}$ potential of Fc/Fc^+ against Ag/Ag^+ in 0.1 M $Bu_4N^+ClO_4^-$/MeCN was detected to be 0.085 V, which was very close to the reported value [64,65]. E_{LUMO} (eV) $= -(E_{red/onset} + 4.88)$ [39,40], where $E_{red/onset}$ value was calibrated against the potential of Fc/Fc^+ pair. E_{HOMO} (eV) $= -(E_{LUMO} + {}^{opt}E_g)$, where $^{opt}E_g$ was obtained from the lowest-energy edge of UV–vis absorption spectra.

2.2. Computational details

The gas-phase geometries of the concerned complexes were optimized without any symmetry restrictions in singlet ground state using the density functional theory (DFT) method at the B3LYP level [41,42]. The 6-31G (d, p) basis set was selected for all the elements. The vibration frequency calculations were performed to ensure that the optimized geometries represented the local minima on the ground-state potential energy surface. All the calculations were carried out with the Gaussian 09 program package in aid of the GaussView visualization program [43]. The absorption spectra based on the B3LYP optimized geometries were stimulated using the time-dependent density functional theory (TD-DFT) and the solvent effect was executed with the polarizable continuum model (PCM) [44,45]. The geometric optimizations of the corresponding excited singlet states were started from the optimized ground-state geometries with the same functional and basis set. The emission spectra were simulated with TD-DFT and PCM methods after the check of the vibration frequencies.

2.3. General procedure for synthesis of ligands **1a**–**f**

At room temperature, diamine (10 mmol) and substituted 2,4-dioxo-butanoate (10 mmol) were added in dioxane (20 mL), the resulted mixture was refluxed overnight to afford the precipitate. After cooling to room temperature, the solid was filtrated and washed with ethanol for several times. The ligand could be recrystallized from ethanol.

1a: 86% yield, yellow powder, m.p. 244.1–244.8 °C; ^{1}H NMR (400 MHz, DMSO-d_6) δ 13.67 (s, 1H), 12.05 (s, 1H), 7.98 (d, $J = 7.3$ Hz, 2H), 7.63–7.47 (m, 4H), 7.15–7.12 (m, 3H), 6.83 (s, 1H); ^{13}C NMR (100 MHz, DMSO-d_6) δ 188.36, 155.66, 145.60, 138.63, 131.81, 128.66, 126.95, 126.71, 124.09, 123.92, 123.60, 116.49, 115.35, 89.14; EI-MS (70 eV) m/z (%) 264 (M^+, 100), 235 (75), 187 (43), 159 (38), 131 (36), 118 (19), 105 (88), 90 (18), 77 (93), 51 (30), 43 (34).

1b: 92% yield, yellow crystal, m.p. 219.8–220.6 °C; ^{1}H NMR (400 MHz, $CDCl_3$) δ 14.06 (s, 1H), 8.04 (d, $J = 7.8$ Hz, 2H), 7.53–7.46 (m, 3H), 7.26–7.21 (m, 3H), 7.16 (t, $J = 7.8$ Hz, 1H), 7.11 (d, $J = 7.2$ Hz, 2H), 7.06 (s, 1H), 6.98 (t, $J = 7.8$ Hz, 1H), 6.57 (d, $J = 8.3$ Hz, 1H), 3.90 (s, 3H); ^{13}C NMR (100 MHz, $CDCl_3$) δ 190.39, 159.98, 156.57, 145.00, 138.88, 131.90, 129.86, 129.39, 128.64, 128.53, 127.44, 125.11, 124.39, 123.53, 116.41, 116.32, 115.51, 91.20, 55.57; EI-MS (70 eV) m/z (%) 370 (M^+, 76), 341 (83), 316 (14), 265 (21), 222 (25), 206 (17), 193 (20), 105 (100), 91 (20), 77 (60), 43 (36).

1c: 83% yield, orange powder, m.p. 217.1–217.5 °C (decomp.); ^{1}H NMR (400 MHz, $CDCl_3$) δ 14.24 (s, 1H), 10.57 (s, 1H), 8.03 (d, $J = 7.1$ Hz, 2H), 7.56–7.43 (m, 3H), 7.19 (d, $J = 8.5$ Hz, 1H), 6.94 (s, 1H), 6.77 (d, $J = 8.9$ Hz, 1H), 6.67 (s, 1H), 3.82 (s, 3H); ^{13}C NMR (100 MHz, DMSO-d_6) δ 185.88, 156.43, 155.76, 145.80, 138.48, 131.57, 128.72, 128.23, 127.01, 126.76, 118.49, 110.43, 99.81, 88.21, 55.43; EI-MS (70 eV) m/z (%) 294 (M^+, 66), 265 (24), 217 (10), 189 (13), 161 (8), 118 (14), 105 (100), 77 (60), 51 (17), 43 (15).

1d: 78% yield, red powder, m.p. 245.7–246.4 °C (decomp.); ^{1}H NMR (400 MHz, DMSO-d_6) δ 14.19 (s, 1H), 12.06 (s, 1H), 8.05–7.91 (m, 2H), 7.65–7.45 (m, 3H), 7.33 (s, 1H), 6.84 (s, 1H), 6.76 (s, 1H), 3.81 (s, 3H), 3.77 (s, 3H); ^{13}C NMR (100 MHz, DMSO-d_6) δ 184.69, 165.73, 155.07, 146.73, 146.40, 145.81, 138.38, 131.36, 128.65, 126.58, 118.06, 101.70, 99.15, 88.23, 55.99, 55.79; EI-MS (70 eV) m/z (%) 324 (M^+, 100), 309 (38), 296 (12), 281 (15), 263 (11), 219 (20), 203 (8), 191 (11), 175 (11), 147 (20), 105 (100), 77 (91), 51 (26), 39 (7).

1e: 85% yield, yellow powder, m.p. 231.2–232.7 °C (decomp.); ^{1}H NMR (400 MHz, DMSO-d_6) δ 13.59 (s, 1H), 12.00 (s, 1H), 7.98 (d, $J = 8.8$ Hz, 2H), 7.48 (d, $J = 3.5$ Hz, 1H), 7.136–7.10 (m, 3H), 7.07 (d, $J = 8.8$ Hz, 2H), 6.79 (s, 1H), 3.85 (s, 3H); ^{13}C NMR (100 MHz, DMSO-d_6) δ 169.79, 163.69, 153.46, 152.08, 130.48, 129.79, 128.18, 124.36, 123.99, 123.87, 121.08, 116.34, 114.79, 89.34, 55.71; EI-MS (70 eV) m/z (%) 294 (M^+, 100), 265 (23), 251 (9), 186 (83), 158 (29), 135 (77), 107 (15), 92 (23), 77 (44), 64 (18), 51 (11), 39 (10).

1f: 73% yield, dark yellow powder, m.p. 232.4–233.0 °C (decomp.); ^{1}H NMR (400 MHz, DMSO-d_6) δ 11.74 (s, 1H), 11.06 (s, 1H), 7.40 (d, $J = 7.6$ Hz, 1H), 7.15–6.95 (m, 3H), 5.50 (s, 1H), 4.16 (q, $J = 7.0$ Hz, 2H), 1.24 (t, $J = 7.1$ Hz, 3H); ^{13}C NMR (100 MHz, DMSO-d_6) δ 169.16, 155.53, 143.93, 125.11, 124.79, 123.36, 122.41, 115.25, 115.16, 83.73, 59.08, 14.28; EI-MS (70 eV) m/z (%) 232 (M^+, 100), 186 (100), 158 (86), 130 (62), 103 (53), 90 (30), 77 (23), 63 (16), 52 (16), 39 (14).

2.4. Synthesis of ligand **1g**

At room temperature and under nitrogen flow, sodium hydride (60 wt% in oil, 1.80 g, 45 mmol) was added to the anhydrous THF solution (30 mL) of 2-methylquinoline (30 mmol, 4.29 g) and ethyl benzoate (40 mmol, 6.0 g). The solution was refluxed for 24 h. After cooling to room temperature, the reaction mixture was added with aq. NH_4Cl and extracted with diethyl ether. The extract was dried over $MgSO_4$ and concentrated in vacuo. Column chromatography of the residue on silica gel gave **1g** (5.26 g, 71%) as a yellow powder.

1g: 73% yield, yellow powder, m.p. 271.4–272.1 °C (decomp.); ^{1}H NMR (400 MHz, $CDCl_3$) δ 15.69 (s, 1H), 7.96 (d, $J = 4.0$ Hz, 2H), 7.61 (d, $J = 9.1$ Hz, 1H), 7.55–7.38 (m, 6H), 7.26–7.21 (m, 1H), 6.83 (d, $J = 9.1$ Hz, 1H), 6.07 (s, 1H); ^{13}C NMR (100 MHz, $CDCl_3$) δ 183.99, 154.04, 139.70, 137.67, 136.07, 130.90, 130.33, 128.21, 127.50, 126.58, 123.61, 123.21, 122.21, 118.05, 89.78; EI-MS (70 eV) m/z (%) 247

(M$^+$, 92), 219 (52), 170 (46), 143 (54), 115 (40), 105 (100), 77 (78), 51 (29), 43 (31), 30 (6).

*2.5. General procedure for synthesis of complexes **2a–g***

At room temperature, triethylamine (5 mmol, 0.505 g, 0.71 mL) was dropped into the suspension of the corresponding ligand (1 mmol) in CH_2Cl_2 (10 mL), the mixture was stirred for 30 min and then boron trifluoride etherate (5 mmol, 0.705 g, 0.63 mL) was added. The resulted mixture was stirred for 12 h and the solid was filtrated. The solid was washed with ether for several times and dried in vacuo. Column chromatography on silica gel gave the complex as a powder or microcrystal.

2a: 88% yield, red powder, m.p. 294.7–295.3 °C; ^{1}H NMR (400 MHz, DMSO-d$_6$) δ 12.88 (s, 1H), 8.14–8.09 (m, 3H), 7.68 (d, $J = 7.4$ Hz, 1H), 7.61 (t, $J = 7.5$ Hz, 2H), 7.51 (t, $J = 7.6$ Hz, 1H), 7.39–7.32 (m, 2H), 7.28 (s, 1H); ^{13}C NMR (100 MHz, DMSO-d$_6$) δ 169.29, 153.40, 152.61, 133.29, 132.13, 130.94, 129.27, 128.76, 127.30, 123.93, 123.82, 121.38, 116.42, 90.45; ^{19}F NMR (376 MHz, DMSO-d$_6$) δ −122.95 (d, $J = 32.1$ Hz); ^{11}B NMR (128 MHz, DMSO-d$_6$) δ 2.74 (s); EI-MS (70 eV) m/z (%) 312 (M$^+$, 100), 283 (70), 247 (12), 219 (12), 179 (17), 142 (12), 105 (52), 90 (12), 77 (64), 51 (17), 45 (37).

2b: 90% yield, orange powder, m.p. 192.5–193.2 °C; ^{1}H NMR (400 MHz, $CDCl_3$) δ 8.45 (d, $J = 8.3$ Hz, 1H), 8.12 (d, $J = 8.0$ Hz, 2H), 7.59 (t, $J = 7.3$ Hz, 1H), 7.51 (t, $J = 7.5$ Hz, 2H), 7.37 (s, 1H), 7.34 (t, $J = 7.8$ Hz, 1H), 7.29–7.23 (m, 3H), 7.15 (d, $J = 8.3$ Hz, 2H), 6.75 (d, $J = 8.3$ Hz, 1H), 3.92 (s, 3H); ^{13}C NMR (100 MHz, $CDCl_3$) δ 172.32, 160.45, 154.04, 151.43, 133.32, 133.06, 132.72, 129.09, 128.89, 128.26, 128.01, 127.85, 125.14, 125.00, 122.74, 116.61, 115.78, 91.35, 55.64; ^{19}F NMR (376 MHz, $CDCl_3$) δ −125.21 (d, $J = 35.7$ Hz); ^{11}B NMR (128 MHz, DMSO-d$_6$) δ 2.24 (s); EI-MS (70 eV) m/z (%) 418 (M$^+$, 51), 389 (18), 370 (78), 341 (74), 265 (19), 222 (27), 206 (14), 193 (22), 105 (100), 77 (81), 63 (12), 51 (20), 39 (6).

2c: 83% yield, red powder, m.p. 294.9–295.4 °C (decomp.); ^{1}H NMR (400 MHz, DMSO-d$_6$) δ 12.84 (s, 2H), 8.11–7.98 (m, 6H), 7.65 (t, $J = 7.2$ Hz, 2H), 7.58 (t, $J = 7.4$ Hz, 4H), 7.25 (t, $J = 7.4$ Hz, 2H), 7.20 (s, 2H), 7.19–7.12 (m, 3H), 7.00 (dd, $J_1 = 7.4$, $J_2 = 2.6$ Hz, 2H), 6.83 (d, $J = 2.6$ Hz, 2H), 3.84 (s, 6H), 2.30 (s, 3H); ^{13}C NMR (100 MHz, DMSO-d$_6$) δ 167.40, 159.36, 153.67, 150.05, 137.33, 132.84, 132.76, 132.37, 129.21, 128.88, 128.18, 126.99, 125.29, 122.98, 118.11, 112.11, 99.31, 90.16, 55.68, 21.02; ^{19}F NMR (376 MHz, DMSO-d$_6$) δ −125.04 (d, $J = 34.1$ Hz); ^{11}B NMR (128 MHz, DMSO-d$_6$) δ 2.15 (s); EI-MS (70 eV) m/z (%) 342 (M$^+$, 64), 313 (12), 105 (60), 91 (100), 77 (37), 45 (42), 39 (21).

2d: 76% yield, dark red powder, m.p. 301.4–302.0 °C (decomp.); ^{1}H NMR (400 MHz, DMSO-d$_6$) δ 12.80 (s, 1H), 7.99 (d, $J = 7.8$ Hz, 2H), 7.74–7.34 (m, 4H), 7.15 (s, 1H), 6.82 (s, 1H), 3.79 (s, 3H), 3.75 (s, 3H); ^{13}C NMR (100 MHz, DMSO-d$_6$) δ 166.81, 153.21, 150.51, 149.67, 145.86, 132.70, 132.45, 129.19, 126.89, 126.61, 117.59, 103.78, 98.42, 90.39, 55.89, 55.86; ^{19}F NMR (376 MHz, DMSO-d$_6$) δ −123.85 (d, $J = 34.9$ Hz); ^{11}B NMR (128 MHz, $CDCl_3$) δ 2.26 (s); EI-MS (70 eV) m/z (%) 372 (M$^+$, 100), 357 (2), 329 (14), 309 (49), 281 (9), 105 (66), 77 (40), 51 (9).

2e: 81% yield, red powder, m.p. 281.5–282.1 °C (decomp.); ^{1}H NMR (400 MHz, DMSO-d$_6$) δ 12.98 (s, 1H), 7.99 (d, $J = 8.8$ Hz, 2H), 7.21–7.14 (m, 2H), 7.12–7.05 (m, 2H), 7.01 (s, 1H), 6.96 (d, $J = 8.8$ Hz, 2H), 3.88 (s, 3H); ^{13}C NMR (100 MHz, DMSO-d$_6$) δ 169.79, 163.67, 153.46, 152.08, 130.48, 129.79, 128.17, 124.36, 123.99, 123.87, 121.08, 116.34, 114.79, 89.34, 55.71; ^{19}F NMR (376 MHz, DMSO-d$_6$) δ −125.02 (d, $J = 33.6$ Hz); ^{11}B NMR (128 MHz, DMSO-d$_6$) δ 2.49 (s); EI-MS (70 eV) m/z (%) 342 (M$^+$, 100), 313 (38), 294 (10), 277 (17), 157 (13), 135 (61), 107 (11), 92(14), 77 (32), 63 (17), 51 (10).

2f: 88% yield, yellow powder, m.p. 172.0–172.5 °C (decomp.); ^{1}H NMR (400 MHz, DMSO-d$_6$) δ 12.53 (s, 1H), 7.84 (d, $J = 8.0$ Hz, 1H), 7.34 (d, $J = 8.0$ Hz, 1H), 7.27–7.23 (m, 2H), 5.91 (s, 1H), 4.48 (q, $J = 7.0$ Hz, 2H), 1.37 (t, $J = 7.0$ Hz, 3H); ^{13}C NMR (100 MHz, DMSO-d$_6$) δ 170.00, 153.55, 153.13, 128.65, 126.38, 124.10, 123.71, 119.57, 116.24, 75.70, 65.84, 14.03; ^{19}F NMR (376 MHz, DMSO-d$_6$) δ −123.54 (d, $J = 34.1$ Hz); ^{11}B NMR (128 MHz, DMSO-d$_6$) δ 2.48 (s); EI-MS (70 eV) m/z (%) 280 (M$^+$, 63), 232 (43), 186 (100), 158 (87), 130 (60), 103 (55), 90(35), 76 (19), 63 (16), 51 (14), 39 (13).

2g: 86% yield, bright yellow crystal, m.p. 230.8–231.6 °C (decomp.); ^{1}H NMR (400 MHz, $CDCl_3$) δ 8.75 (d, $J = 8.7$ Hz, 1H), 8.16 (d, $J = 8.7$ Hz, 1H), 8.02 (d, $J = 7.6$ Hz, 2H), 7.80 (t, $J = 8.0$ Hz, 1H), 7.76 (d, $J = 7.9$ Hz, 1H), 7.54 (t, $J = 7.5$ Hz, 1H), 7.51–7.44 (m, 3H), 7.25 (d, $J = 9.6$ Hz, 1H), 6.42 (s, 1H); ^{13}C NMR (100 MHz, $CDCl_3$) δ 164.99, 153.96, 141.25, 139.52, 133.52, 132.43, 131.52, 128.58, 128.41, 126.84, 126.64, 126.49, 122.95, 121.13, 94.02; ^{19}F NMR (376 MHz, $CDCl_3$) δ −126.79 (q, $J = 18.8$ Hz); ^{11}B NMR (128 MHz, DMSO-d$_6$) δ 2.52 (t, $J = 19.2$ Hz); EI-MS (70 eV) m/z (%) 294 ((M − 1)$^+$, 100), 274 (12), 230 (23), 115 (21), 101 (8), 77 (28), 51 (15), 39 (7).

3. Results and discussion

*3.1. Synthesis of complexes **2a–g***

The synthetic routes to BF_2 complexes **2a–g** are illustrated in Scheme 1. The dioxane solutions of *o*-phenylenediamines and

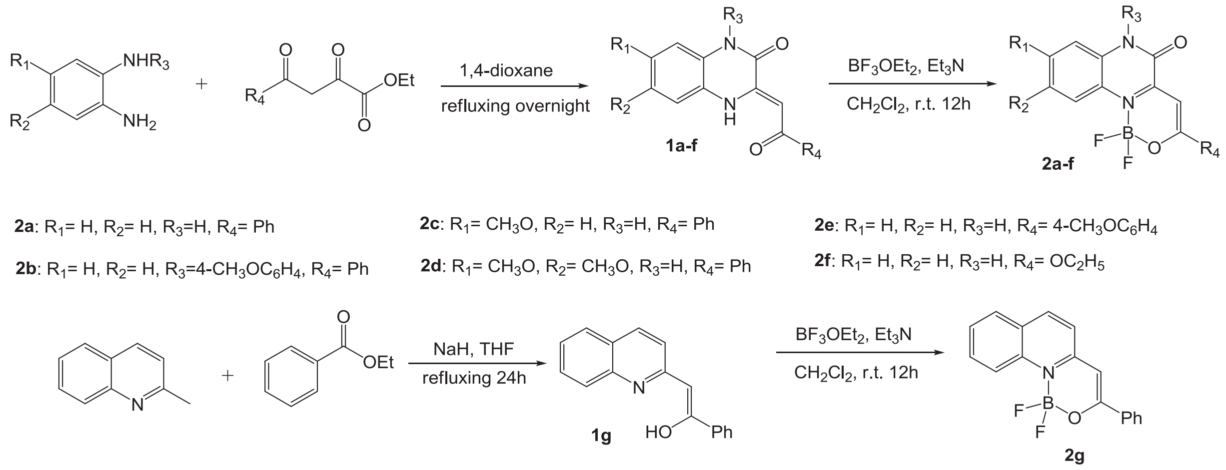

Scheme 1. The synthetic routes to BF_2 complexes.

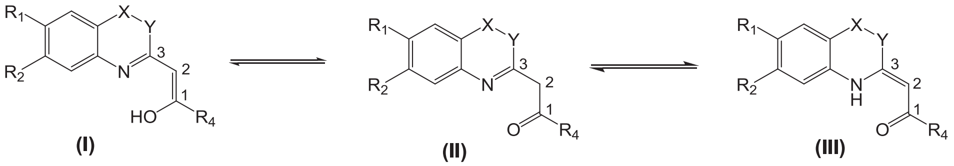

Scheme 2. The tautomeric equilibrium of ligands **1a**–**g**.

2,4-dioxo-butanoates are refluxed overnight without any catalyst to offer the ligands **1a**–**f** as the precipitates. A Claisen ester-condensation is taken place when 2-methylquinoline subsequently reacts with ethyl benzoate in the presence of sodium hydride, providing the ligand **1g** as a yellow solid. The preparation of the complexes **2a**–**g** can be readily accomplished in good to excellent yields by treating the ligands with excessive trifluoroboron etherate under the basic condition. These BF_2 complexes can be well dissolved in many solvents and stored in solid state under the atmosphere for several months with the negligible decomposition.

3.2. NMR spectra study

Theoretically, there are three tautomers for a parent ligand, they are enolimine (**I**), ketoimine (**II**) and ketoenamine (**III**) (Scheme 2). However, both the ^1H and the ^{13}C NMR spectra clearly demonstrate that only a sole tautomer exists in the solution of a given ligand. For **1g**, only 1-phenyl-2-(quinolin-2-yl)ethanol, the enolimine tautomer, can be detected in the $CDCl_3$ solution. The ketoimine tautomer can be completely excluded since its characteristic resonance of methylene H_2 atoms in the 4–5 ppm region is unobservable. Moreover, it is safe to announce that a ketoenamine tautomer is impossible to occur in the solution of **1g** since the destruction of an aromatic system is unreasonable. For **1a**–**f**, the existence of ketoimines can also be entirely eliminated due to the absence of the methylene H_2 signals in the 3–4 ppm region. The lack of the methylene C_2 chemical shifts at ~50 ppm on the ^{13}C NMR spectra is the other evidence for the elimination of ketoimines. It seems that ketoenamines are more likely to be existent than enolimines in solutions of **1a**–**f**, as the relatively low-field ^1H NMR signals at ~14 ppm can be ascribed to the formation of the intramolecular hydrogen bonds between the oxygen atoms on the keto carbonyls and the active protons on the enamino [46]. The DFT calculations test the above assumption and reveal that ketoenamines are more thermodynamically preferred than enolimines. As for **1a**, 3-(2-oxo-2-phenylethylidene)-3,4-dihydroquinoxalin-2(1H)-one (ketoenamine) is more stable than 3-(2-hydroxy-2-phenylvinyl)quinoxalin-2(1H)-one (enolimine) by 0.477 kcal/mol in the DMSO solution at 25 °C.

On the ^1H NMR spectra, the most obvious variation between a ligand and its corresponding BF_2 chelate is the disappearance of the proton signal in the lowest-field region. Additionally, due to the chelation with BF_2 group, the proton signals go through a different extent down-field shift from a parent ligand to its complex. On the ^{13}C NMR spectra, a remarkably shielding effect occurs on the C_1 atom owning to its transformation from a carbonyl to an enol. Thus, a considerably up-field shift of the C_1 signal takes place from ~190 ppm in a parent ligand to ~165 ppm in its BF_2 complex.

The striking difference between **2a**–**f** and **2g** occurs on the ^{11}B and the ^{19}F NMR spectra (Fig. 1). For **2g**, its ^{11}B and ^{19}F NMR exhibit a well-resolved triplet and a quartet resonance respectively. It is assumed that a fast ring-flipping process which results in an exchange-averaged conformation with the symmetrically equivalent fluorines might be responsible for the NMR performances of **2g** in solutions [47]. For each of **2a**–**f**, however, a broad singlet signal of ^{11}B and a doublet signal of ^{19}F can be observed. Actually, these signals should be considered as the poor-resolved triplet and quartet resonances. This dramatically diminished resolution is presumably caused by the ultrafast ring-flipping process in solutions. Obviously, the frequency of the ring-flipping is related to the structure of a complex.

3.3. Photophysical feature

In general, an excellent mirror-image relationship with the fine vibrations between the absorption and the emission spectra can be observable for each complex, which implies that the vibration levels in the S_1 state are similar to those in the S_0 state [48]. The spectra of **2a** and **2g** are selected to be illustrated in Fig. 2. Furthermore, the high molar extinction coefficients of these complexes suggest that permitted π–π^* transitions occur in the process of excitation. They display the intensely multicolor fluorescence in solutions. The photos of them in the CH_2Cl_2 solution under a hand-held ultraviolet lamp are shown in Fig. 3.

It is found that a qualitative correlation between the optical properties and the molecular structures can be connected among these BF_2 complexes (Table 1). When the benzoyl in **2a** is substituted by the carbethoxyl in **2f**, a substantially hypsochromic

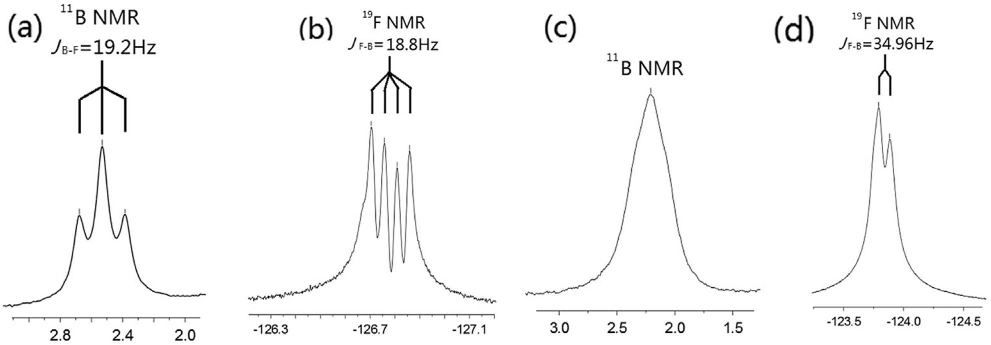

Fig. 1. ^{11}B NMR spectra of **2g** (a) and **2d** (c) along with ^{19}F NMR spectra of **2g** (b) and **2d** (d).

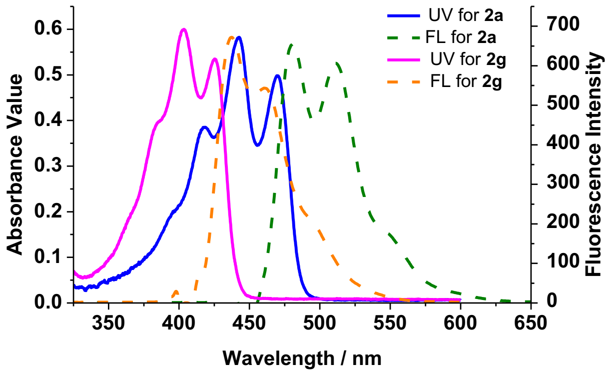

Fig. 2. Normalized spectra of complex **2a** and **2g** (solid lines for absorption and dash lines for emission).

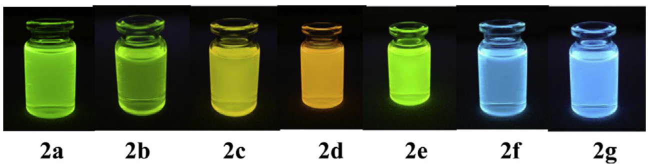

Fig. 3. Photos of complex **2a**–**g** in CH_2Cl_2 solution under a hand-hold 365 nm ultraviolet lamp.

shift of the spectral maxima along with the remarkable decrease of the molar extinction coefficient occur. Such difference of their optical behaviors should be attributed to the reduced electronic density on the N–B–O chromophore from in **2a** to in **2f**. Similarly, when the quinolinyl ring in **2g** replaces the quinoxalinone ring in **2a**, the spectra of the former go through a strikingly blue shift. Clearly, the amide group in **2a** makes a large contribution to the long-wavelength absorption and emission.

Additionally, when a methoxyl is located on either the benzoyl or the quinoxalinone moiety, the spectra of the corresponding complex exhibit a bathochromic shift in comparison with those of **2a**. For **2c** where a methoxyl is introduced on the quinoxalinone moiety, its spectra have the larger red shifts than those of **2e** where a methoxyl is attached on the benzoyl moiety. However, **2c** has the lower molar extinction coefficient than that of **2e**. Although **2d** shows the much larger red shifts than **2a** in the spectral maxima, the former has the decreased molar extinction coefficient than that of the latter. It is suggested that a molecular bend caused by the steric hindrance between the two vicinal methoxyl groups on the quinoxalinone moiety may account for the decreased molar extinction coefficient of **2d** [33,49,50].

The investigation of **2b** reveals that its photophysical performance is almost identical to that of **2a**. This demonstrates that the imposing of a *p*-methoxylphenyl group onto the amide moiety has little dedication to the extension of π-conjugation. This assumption is tested to be reasonable by the DFT calculation of **2b**.

Complex **2a** and **2g** are selected to survey the solvent effect on their optical behaviors. It is indicated in Table 2 that both their UV–vis and fluorescent spectra are insensitive to the solvatochromism. Not only the maxima but also the quantum yields have the minute response to the variation of solvent polarity. This solvent-independent optical property infers that an intramolecular charge transfer (ICT) excited state can barely exist in the photo-induced excitation [51–54]. This presumption is also verified to be reliable by the time-dependent density functional theory (TD-DFT) calculations.

3.4. Electrochemical behaviors

It was reported by the previous research that BODIPYs are good electron acceptors [55]. Therefore, our *N,O*-bidentate BF_2 complexes, which are the cousins of BODIPYs, are expected to have good electron-accepting abilities. The electrochemical behaviors of **2a** and **2f** along with those of **1a** and **1f** are investigated by the cyclic voltammetry (CV).

It is observed that the onset reduction potentials of **2a** and **2f** undergo the considerably positive shifts in comparison with those of **1a** and **1f**. The onset reduction potentials of **2a** and **2f** are −1.22 V and −1.55 V respectively while those of **1a** and **1f** are −1.66 V and −1.96 V respectively. Such positive shift in reduction potentials from a ligand to a BF_2 complex is similar to the case of the *N,O*-bidentate BF_2 chelates with perylene tetracarboxlic diimide ligands [56]. The relatively positive reduction potential of a complex indicates that a large decrease of the electronic density happens on it due to the chelation of BF_2 group.

The electronic states (HOMO/LUMO levels) of **2a**–**g** are investigated by CV. The recorded CV curves (Fig. 4(A)) demonstrate that

Table 1
Photophysical properties of *N,O*-chelated BF_2 complexes.

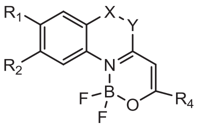

Complex	R_1	R_2	R_4	X	Y	Dicholoromethane[a]				
						λ_{ab} (nm)	λ_{em} (nm)	ε ($\times 10^4$ M^{-1} cm^{-1})[b]	f[c]	Φ_f[d]
2a	H	H	C_6H_5	NH	C=O	419, $\underline{442}$, 470	481, 512	4.09	0.8253	0.64
2b	H	H	C_6H_5	4-$CH_3OC_6H_4NH$	C=O	419, $\underline{445}$, 472	482, 515	4.20	0.8461	0.59
2c	CH_3O	H	C_6H_5	NH	C=O	438, $\underline{460}$, 490	505, 534	4.28	0.8390	0.74
2d	CH_3O	CH_3O	C_6H_5	NH	C=O	$\underline{483}$, 514	541	3.62	0.7019	0.71
2e	H	H	4-$CH_3OC_6H_4$	NH	C=O	428, $\underline{451}$, 481	493, 523	4.97	1.0222	0.66
2f	H	H	OC_2H_5	NH	C=O	379, $\underline{400}$, 426	437, 460	2.25	0.5286	0.46
2g	H	H	C_6H_5	=CH	=CH	$\underline{403}$, 425	437, 461	3.12	0.8415	0.84

[a] Measured in 1.0×10^{-5} mol/L at 25 °C.
[b] Measured at the underlined wavelength.
[c] Oscillator strength of the absorptions obtained with TD-DFT–PCM calculations at B3LYP level with 6-31G (d,p) basis set.
[d] Using quinine sulfate ($\Phi_f = 0.55$ in 0.5 mol/L H_2SO_4 aqueous solution) as the standard for **2f**–**g** while using fluorescein ($\Phi_f = 0.91$ in 0.1 mol/L NaOH aqueous solution) as the standard for **2a**–**e**.

Table 2
Solvent effect on complex **2a** and **2g**.

Solvent	Complex **2a**			Complex **2g**		
	λ_{ab} (nm)	λ_{em} (nm)	$\Phi/\Phi_{CH_2Cl_2}$	λ_{ab} (nm)	λ_{em} (nm)	$\Phi/\Phi_{CH_2Cl_2}$
Benzene	422, 447, 474	482, 513	0.94	386, 406, 429	440, 463	0.99
$CHCl_3$	419, 444, 471	483, 514	0.99	387, 404, 427	436, 462	0.96
EtOAc	421, 442, 469	482, 513	0.96	386, 402, 423	436, 462	0.94
THF	420, 443, 468	480, 515	1.03	387, 403, 425	439, 461	1.03
CH_2Cl_2	419, 442, 470	481, 512	1.00	386, 403, 425	438, 461	1.00
$(CH_3)_2CO$	421, 444, 472	483, 515	0.93	384, 400, 421	437, 460	0.99
CH_3OH	424, 446, 477	485, 520	0.91	384, 401, 422	436, 459	1.00
CH_3CN	421, 445, 478	484, 523	0.95	382, 399, 419	438, 460	0.93
DMSO	422, 444, 478	485, 521	1.05	384, 404, 426	443, 464	1.04

there is a reversible one-electron reduction wave for each complex except **2c** and each complex has an irreversible oxidation wave. There are many reports in literature that the optical energy gap obtained from the lowest-energy edge of UV–vis absorption spectra can be used to replace the electrochemical energy gap in estimation of the absolute HOMO or LUMO levels [59,60], as these two energy gaps are always quite close to each other [27,62,63]. For complex **2a**–**g**, each LUMO level is determined by the onset reduction potential based on the standard reduction waves. However, due to the existence of some unknown small peaks on the oxidation waves for several complexes, the accurate onset oxidation potentials become hard to be determined. Therefore, the HOMO levels are estimated with the optical energy gaps and the results are listed in Table 3.

It is indicated that both the HOMO and the LUMO levels are enhanced for **2c** and **2d** where one and two methoxyl groups are located at the quinoxalinone moiety, compared with those of **2e** whose methoxyl group is imposed at the benzoyl moiety. However, the enhancement of the HOMO levels makes the more contribution to the reduced energy gaps of **2c** and **2d** than that of the LUMO levels. Similarly, owning to the shortage of the π-conjugation devoted by the *p*-methoxylphenyl group, the electrochemical performance of **2b** is almost identical to that of **2a**. For **2f** and **2g**, it is investigated that they show the much lower reduction potentials and higher LUMO levels than those of **2a**–**e**. The greatly enhanced LUMO levels should be responsible for the enlarged energy gaps of **2f** and **2g**. Fig. 4(B) clearly illustrates the relationship of the frontier MOs among these complexes.

The electrochemical data show that the LUMO levels of our complexes are lower than that of 1,3,5,7-tetramethyl-8-phenyl-BODIPY (−3.05 eV) [27,32] which is a widely used BODIPY derivative and the commonly used electron-transport material Alq_3 (−3.0 eV) [57]. These comparisons suggest that our BF_2 chelates have the better electron-accepting capability than them.

3.5. *Theoretical study*

For the better understanding of the optical and electrochemical properties displayed by **2a**–**f**, the DFT calculations are performed under the polarizable continuum model (PCM) at the B3LYP level, using the 6-31G (d,p) basis set for all atoms.

Complex **2f** is chosen as an example to compare the simulated and the experimental spectra (Fig. 5). Although the short-wavelength regions cannot be acquired due to the limitations in the instrument, the measured spectra are in good agreement with the calculated ones in the long-wavelength regions. Regardless of the fine vibrations, the calculated maxima are very close to the experimental ones.

Table 3
Electrochemical data for complex **2a**–**g** (vs Ag/Ag^+) in anhydrous acetonitrile and HOMO–LUMO gaps determined from spectroscopy and TD-DFT calculations.

Comp	$E_{red/onset}$[a] (V)	E_{HOMO}[b] (eV)	E_{LUMO}[b] (eV)	$^{opt}E_g$[c] (eV)	E_{HOMO}[d] (eV)	E_{LUMO}[d] (eV)	$^{Cal}E_g$[d] (eV)
2a	−1.22	−6.23	−3.66	2.57	−6.35	−3.14	3.21
2b	−1.21	−6.23	−3.67	2.56	−6.27	−3.08	3.19
2c	−1.28	−6.04	−3.60	2.44	−5.75	−2.70	3.05
2d	−1.31	−5.89	−3.57	2.32	−5.48	−2.64	2.84
2e	−1.23	−6.17	−3.65	2.52	−5.81	−2.65	3.16
2f	−1.55	−6.18	−3.33	2.85	−6.21	−2.64	3.57
2g	−1.63	−6.20	−3.25	2.85	−6.18	−2.65	3.59

[a] Calibrated $E_{red/onset}$ with Fc/Fc^+ as the internal standard.
[b] E_{LUMO} (eV) = $-(E_{red/onset} + 4.88)$, E_{HOMO} (eV) = $-(E_{LUMO} + {}^{opt}E_g)$.
[c] Calculated by lowest-energy edge of absorption spectra.
[d] Obtained by MO calculations in acetonitrile.

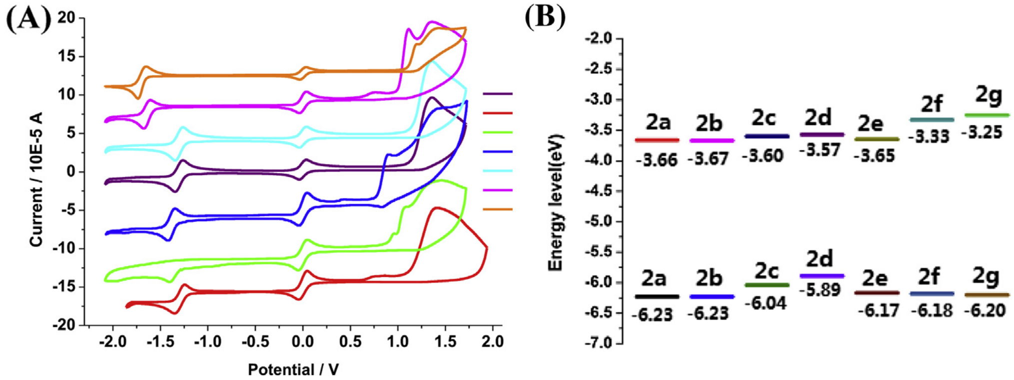

Fig. 4. (A) Cyclic voltammograms for **2a**–**g** (The wave at 0 V potential corresponds to Fc/Fc^+ pair. All voltammograms are calibrated to the ferrocene anodic peak.); (B) Diagram on HOMO and LUMO energy level of **2a**–**g**.

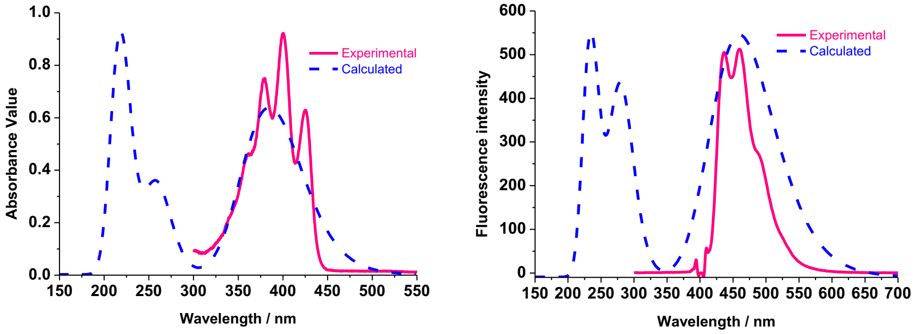

Fig. 5. Normalized absorption and emission spectra of **2f** (solid lines for the experimental curves and dash lines for the simulated curves).

Complex **2a**, **2f** and **2g** are screened as the candidates to run the calculations so that the deep insight of their transition features can be afforded. It is indicated in Table 4 that both the excitation and the radiation transitions between the S_0 and the S_1 state are dominantly contributed by the HOMO and the LUMO of each complex. In the low-lying electronic states of these complexes, it is easy to judge from the oscillator strengths that the S_2 states are the “dark” S_2 states in which the involved absorptions and the emissions are prohibited. There is a general assumption that the red shift emission is related to the enlarged dipole moment in the excited state [58], as an excited state with the enlarged dipole moment can be more stabilized in a polar solvent than a ground state. Consequently, a tiny change of the dipole moments between the ground and the excited state usually leads to the little solvatochrimism. The data in Table 4 demonstrate that there is a minute variation of the dipole moments between the S_0 and the S_1 state for each examined complex. Hence, the nature for the solvent-insensitive optical behaviors of these complexes is clearly revealed by the theoretical calculations.

The visualized HOMOs and LUMOs of **2a**, **2b**, **2f** and **2g** are illustrated in Fig. 6. Evidently, the distribution of the HOMO and the LUMO in **2a**, **2f** and **2g** is approximately donated by the atomic orbitals throughout the whole molecule. For both the HOMO and the LUMO of **2b**, however, the electrons are completely excluded from the *p*-methoxylphenyl moiety. Such exclusion results in the absence of the π-conjugation participated by the *p*-methoxylphenyl moiety. Consequently, the optical and the electrochemical properties of **2b** are almost identical to those of **2a**. For each of the calculated complexes, the ICT transition rarely occurs in the photo-induced excitation and the transition from the HOMO to the LUMO should be assigned to a $\pi-\pi^*$ transition.

The calculated HOMO and LUMO levels of **2a**–**g** are listed in Table 3. It is indicated that the calculated HOMO levels are in good agreement with those obtained from the measured optical energy gaps, but the computed LUMO levels are considerably overestimated. This overestimation of LUMO levels is very common for the DFT calculations [27,59,60]. In spite of this overestimation, the trend of HOMO-LUMO energy gaps in the theoretic study is still entirely consistent with that in the experimental investigation. By reference to **2a**, the reduced energy gaps of **2c**–**e** predominantly derive from the increase of the HOMO levels due to the extension of the conjugated regions, while the enlarged energy gaps of **2f**–**g** mainly result from the enhancement of the LUMO levels owning to the diminished electron density on the N–B–O chromophores. These calculation outcomes reasonably account for the spectral performance of these BF_2 chelates.

Usually, homologous compounds have the structure-reliant oscillator strengths [61]. Considering **2a**–**f** as a system, it is indicated in Table 1 that **2e** which has a methoxyl group at the benzoyl moiety has the largest oscillator strength, but **2f** where a carbethoxyl takes the place of a benzoyl has the smallest one. The trend of the calculated oscillator strengths among these complexes is in perfect accordance with that of the measured molar extinction coefficients. In term of **2g** whose chemical structure is substantially

Table 4
Selected electronic transition energies and corresponding oscillator strengths (*f*), main compositions and CI coefficients of the low-lying electronic excited states of complex **2a**, **2f**, **2g**.

Complex	Dipole moment (*D*)	Electronic transition	TD-DFT/PCM/B3LYP/6-31G (d, p) (in CH_2Cl_2)			
			Energy (eV)	Oscillator strength (*f*)	Composition	CI
2a	4.033 (S_0) 3.836 (S_1)	$S_0 \rightarrow S_1$	2.84 (437 nm)	0.8484	H → L	0.7054
		$S_0 \rightarrow S_2$	3.33 (372 nm)	0.0489	H-1 → L	0.7000
		$S_1 \rightarrow S_0$	2.51 (494 nm)	0.8287	L → H	0.7080
		$S_2 \rightarrow S_0$	3.09 (401 nm)	0.0429	L → H-1	0.7008
2f	1.527 (S_0) 1.307 (S_1)	$S_0 \rightarrow S_1$	3.22 (385 nm)	0.5500	H → L	0.7036
		$S_0 \rightarrow S_2$	3.73 (332 nm)	0.0091	H-1 → L	0.6981
		$S_1 \rightarrow S_0$	2.69 (461 nm)	0.4420	L → H	0.6996
		$S_2 \rightarrow S_0$	3.02 (411 nm)	0.0143	L → H-3	0.1190
					L → H-1	0.6861
2g	7.570 (S_0) 7.512 (S_1)	$S_0 \rightarrow S_1$	3.11 (399 nm)	0.8250	H → L	0.7034
		$S_0 \rightarrow S_2$	3.80 (327 nm)	0.0075	H-1 → L	0.6580
					H → L + 1	0.2331
		$S_1 \rightarrow S_0$	2.70 (460 nm)	0.5690	L → H	0.6943
					L + 1 → H	0.1110
		$S_2 \rightarrow S_0$	3.35 (370 nm)	0.0092	L → H-1	0.5949
					L + 1 → H-1	0.1181
					L + 1 → H	0.3351

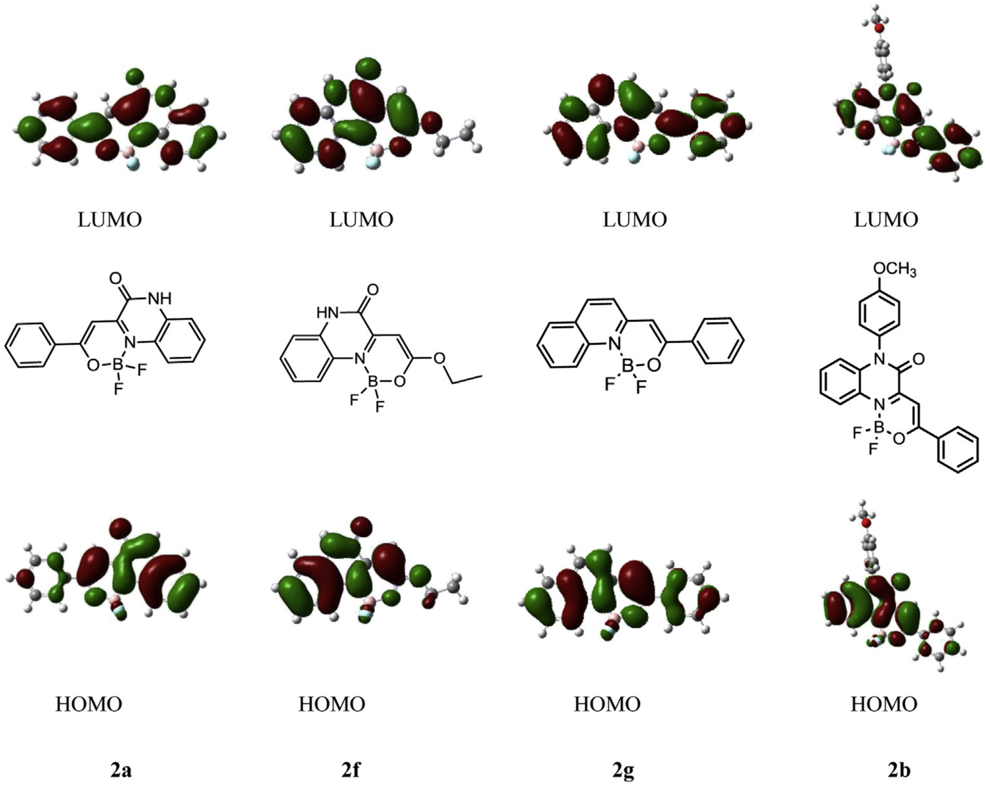

Fig. 6. The selected frontier molecular orbitals of complex **2a**, **2f**, **2g** and **2b**.

Table 5
Selected electronic transition energies and corresponding oscillator strengths (*f*), main compositions and CI coefficients of the lowest electronic excited states of complex **2f**.

Solvent	Dipole moment (*D*)	Electronic transition	TD-DFT/PCM/B3LYP/6-31G (d, p)			
			Energy (eV)	Oscillator strength (*f*)	Composition	CI
Benzene	1.235 (S_0)	$S_0 \rightarrow S_1$	3.21 (386 nm)	0.5572	H → L	0.70377
	1.031 (S_1)	$S_1 \rightarrow S_0$	2.76 (450 nm)	0.5092	L → H	0.70737
Dichloromethane	1.527 (S_0)	$S_0 \rightarrow S_1$	3.22 (385 nm)	0.5500	H → L	0.70362
	1.307 (S_1)	$S_1 \rightarrow S_0$	2.69 (461 nm)	0.4420	L → H	0.69957
Acetonitrile	1.722 (S_0)	$S_0 \rightarrow S_1$	3.23 (384 nm)	0.5286	H → L	0.70321
	1.425 (S_1)	$S_1 \rightarrow S_0$	2.78 (446 nm)	0.4874	L → H	0.70734

distinct from that of **2a**, no correlation between their oscillator strengths and molar extinction coefficients can be connected.

Taking **2f** as an example, we examine the solvent effect on the dipole moments and the results are listed in Table 5. It is found that the dipole moments of the S_1 and the S_0 state are increased as the solvent polarity is enhanced, but the dipole moment of the excited state is slightly smaller than that of the ground state in each of the tested solvents. The minute difference of the dipole moments between the S_0 and the S_1 state in different solvents implies that the transitions of **2f** should be solvent-independent. Actually, the spectral maxima, oscillator strengths, main compositions and CI coefficients are all insensitive to the solvent polarity.

4. Conclusion

Herein we describe the synthesis along with the property and the calculation study on a series of novel BF_2 complexes with *N*,*O*-bidentate ligands. These complexes are ready to be prepared in good yields by simple operation and exhibit intense fluorescence in solutions with multiple colors. A qualitative structure–property correlation has been established via the detailed measurements and verified by the DFT calculations. It is revealed that (i) the dramatically blue-shifted spectral bands along with the substantially decreased molar extinction coefficient occur if a benzoyl is substituted by a carbethoxy on a complex; (ii) the amide moiety makes a large contribution for the long-wavelength fluorescence of complexes, but the substituent on the amide moiety is barely helpful for the extension of the π-conjugation; (iii) a complex with an electron-donating group at the quinoxalinone moiety has the larger red shifts of spectral bands and the less stability toward oxidation than the one with an electron-donating group at the benzoyl moiety; (iv) the increase of the HOMO levels may account for the long-wavelength emission while the short-wavelength fluorescence may be caused by the enhancement of the LUMO levels; and (v) these BF_2 chelates have the solvent-independent photophysical performance due to the minute change of the dipole moments between the S_0 and the S_1 state.

Moreover, the electrochemical investigation shows that these novel *N*,*O*-bidentate BF_2 chelates are better electron acceptors than the commonly used electron-transport material Alq_3. The further research on exploiting them as electron-transporting materials is on the progress.

Acknowledgments

We are grateful for the financial support of the Natural Science Foundation of Zhejiang Province (Y4100034) and Zhejiang Province Key Innovation Team (2012R 10038-09).

Appendix A. Supplementary data

Supplementary data related to this article can be found at http://dx.doi.org/10.1016/j.jorganchem.2013.06.012.

References

[1] A.C. Benniston, G. Copley, Phys. Chem. Chem. Phys. 11 (2009) 4124–4131.
[2] R. Ziessel, G. Ulricha, A. Harrimanb, New J. Chem. 31 (2007) 496–501.
[3] G. Ulrich, R. Ziessel, Anthony Harriman, Angew. Chem. Int. Ed. 47 (2008) 1184–1201.
[4] X. Zhang, H.-S. Zhang, Spectrochim. Acta A 61 (2005) 1045–1049.
[5] T. Matsumoto, Y. Urano, T. Shoda, H. Kojima, T. Nagano, Org. Lett. 9 (2007) 3375–3377.
[6] X. Peng, J. Du, J. Fan, J. Wang, Y. Wu, J. Zhao, S. Sun, T. Xu, J. Am. Chem. Soc. 129 (2009) 1500–1501.
[7] A. Coskun, M.D. Yilmaz, E.U. Akkaya, Org. Lett. 9 (2007) 607–609.
[8] M. Baruah, W. Qin, R.A.L. Valle′e, D. Beljonne, T. Rohand, W. Dehaen, N. Boens, Org. Lett. 7 (2005) 4377–4380.
[9] J.-P. Malval, I. Leray, B. Valeur, New J. Chem. 29 (2005) 1089–1094.
[10] R. Ziessel, G. Ulrich, A. Harriman, M.A.H. Alamiry, B. Stewart, P. Retailleau, Chem. Eur. J. 15 (2009) 1359–1369.
[11] C.F.A. Gómez-Durán, I. García-Moreno, A. Costela, V. Martin, R. Sastre, J. Bañuelos, F. López Arbeloa, I. López Arbeloa, E. Peña-Cabrera, Chem. Commun. 46 (2010) 5103–5105.
[12] M.J. Ortiz, I. Garcia-Moreno, A.R. Agarrabeitia, G. Duran-Sampedro, A. Costela, R. Sastre, F. López Arbeloa, J. Bañuelos Prieto, I. López Arbeloa, Phys. Chem. Chem. Phys. 12 (2010) 7804–7811.
[13] S. Ertan-Ela, M.D. Yilmaz, B. Icli, Y. Dede, S. Icli, E.U. Akkaya, Org. Lett. 10 (2008) 3299–3302.
[14] T. Rousseau, A. Cravino, T. Bura, G. Ulrich, R. Ziessel, J. Roncali, Chem. Commun. (2009) 1673–1675.
[15] M.K. Kuimova, G. Yahioglu, J.A. Levitt, K. Suhling, J. Am. Chem. Soc. 130 (2008) 6672–6673.
[16] M.A.H. Alamiry, A.C. Benniston, G. Copley, K.J. Elliott, A. Harriman, B. Stewart, Y.-G. Zhi, Chem. Mater. 20 (2008) 4024–4032.
[17] J.F. Lovell, T.W.B. Liu, J. Chen, G. Zheng, Chem. Rev. 110 (2010) 2839–2857.
[18] S. Ozlem, E.U. Akkaya, J. Am. Chem. Soc. 131 (2009) 48–49.
[19] Y. Kubota, Y. Tsuzuki, K. Funabiki, M. Ebihara, M. Matsui, Org. Lett. 12 (2010) 4010–4013.
[20] J. Bañuelos, F. López Arbeloa, V. Martinez, M. Liras, A. Costela, I. García Moreno, I. López Arbeloa, Phys. Chem. Chem. Phys. 13 (2011) 3437–3445.
[21] M.F. Mao, S.Z. Xiao, T. Yi, K. Zou, J. Fluorine Chem. 132 (2011) 612–616.
[22] Q. Cao, S.Z. Xiao, M.F. Mao, X.H. Chen, S. Wang, L. Li, K. Zou, J. Organometal. Chem. 717 (2012) 147–151.
[23] M.F. Mao, S.Z. Xiao, J.F. Li, Y. Zou, R.H. Zhang, J.R. Pan, F.J. Dan, K. Zou, T. Yi, Tetrahedron 68 (2012) 5037–5041.
[24] A. Esparza-Ruiz, A. Peña-Hueso, H. Nöth, A. Flores-Parra, R. Contreras, J. Organometal. Chem. 694 (2009) 3814–3822.
[25] K. Perumal, J.A. Garg, O. Blacque, R. Saiganesh, S. Kabilan, K.K. Balasubramanian, K. Venkatesan, Chem. Asian J. 7 (2012) 2670–2677.
[26] H.J. Li, W.-F. Fu, L. Li, X. Gan, W.-H. Mu, W.-Q. Chen, X.-M. Duan, H.-B. Song, Org. Lett. 12 (2010) 2924–2927.
[27] Y. Zhou, Y. Xiao, D. Li, M.-Y. Fu, X.-H. Qian, J. Org. Chem. 73 (2008) 1571–1574.
[28] G.M. Fischer, E. Daltrozzo, A. Zumbusch, Angew. Chem. Int. Ed. 50 (2011) 1406–1409.
[29] F. Ito, T. Nagai, Y. Ono, K. Yamaguchi, H. Furuta, T. Nagamura, Chem. Phys. Lett. 435 (2007) 283–288.
[30] Y. Yang, X. Su, C.N. Carroll, I. Aprahamian, Chem. Sci. 3 (2012) 610–613.
[31] Y.-Y. Wu, Y. Chen, G.-Z. Gou, W.-H. Mu, X.-J. Lv, M.-L. Du, W.F. Fu, Org. Lett. 14 (2012) 5226–5229.
[32] Y. Zhou, Y. Xiao, S.-M. Chi, X.-H. Qian, Org. Lett. 10 (2008) 633–636.
[33] Y. Kubota, H. Hara, S. Tanaka, K. Funabiki, M. Matsui, Org. Lett. 13 (2011) 6544–6547.
[34] Y. Zhou, J.W. Kim, M.J. Kim, W.-J. Son, S.J. Han, H.N. Kim, S. Han, Y. Kim, C. Lee, S.-J. Kim, D.H. Kim, J.-J. Kim, J. Yoon, Org. Lett. 12 (2010) 1272–1275.
[35] R.-Z. Ma, Q.-C. Yao, X. Yang, M. Xia, J. Fluorine Chem. 137 (2012) 93–98.
[36] Y. Kubota, S. Tanaka, K. Funabiki, M. Matsui, Org. Lett. 14 (2012) 4682–4685.
[37] M. Xia, B. Wu, G.F. Xiang, J. Fluorine Chem. 129 (2008) 402–408.
[38] Z.B. Henson, G.C. Welch, T. van der Poll, G.C. Bazan, J. Am. Chem. Soc. 134 (2012) 3766–3799.
[39] Y. Liang, Y. Wu, D. Feng, S.-T. Tsai, H.-J. Son, G. Li, L. Yu, J. Am. Chem. Soc. 131 (2009) 56–57.
[40] Y. Kubo, K. Watanabe, R. Nishiyabu, R. Hata, A. Murakami, T. Shoda, H. Ota, Org. Lett. 13 (2011) 4574–4577.
[41] A.D. Becke, J. Chem. Phys. 98 (1993) 5648–5652.
[42] C. Lee, W. Yang, R.G. Parr, Phys. Rev. B 37 (1988) 785–789.
[43] M.J. Frisch, G.W. Trucks, H.B. Schlegel, G.E. Scuseria, M.A. Robb, J.R. Cheeseman, G. Scalmani, V. Barone, B. Mennucci, G.A. Petersson, H. Nakatsuji, M. Caricato, X. Li, H.P. Hratchian, A.F. Izmaylov, J. Bloino, G. Zheng, J.L. Sonnenberg, M. Hada, M. Ehara, K. Toyota, R. Fukuda, J. Hasegawa, M. Ishida, T. Nakajima, Y. Honda, O. Kitao, H. Nakai, T. Vreven, J.A. Montgomery Jr., J.E. Peralta, F. Ogliaro, M. Bearpark, J.J. Heyd, E. Brothers, K.N. Kudin, V.N. Staroverov, R. Kobayashi, J. Normand, K. Raghavachari, A. Rendell, J.C. Burant, S.S. Iyengar, J. Tomasi, M. Cossi, N. Rega, J.M. Millam, M. Klene, J.E. Knox, J.B. Cross, V. Bakken, C. Adamo, J. Jaramillo, R. Gomperts, R.E. Stratmann, O. Yazyev, A.J. Austin, R. Cammi, C. Pomelli, J.W. Ochterski, R.L. Martin, K. Morokuma, V.G. Zakrzewski, G.A. Voth, P. Salvador, J.J. Dannenberg, S. Dapprich, A.D. Daniels, O. Farkas, J.B. Foresman, J.V. Ortiz, J. Cioslowski, D.J. Fox, Gaussian 09, Revision A.02, Gaussian, Inc., Wallingford CT, 2009.
[44] M. Cossi, N. Rega, G. Scalmani, V. Barone, J. Comput. Chem. 24 (2003) 669–681.
[45] N.M. O'Boyle, A.L. Tenderholt, K.M. Langner, J. Comput. Chem. 29 (2008) 839–845.
[46] L.-X. Wu, K. Burgess, J. Am. Chem. Soc. 130 (2008) 4089–4096.
[47] P.M. Felipe, C. Gwengo, S.V. Lindeman, M.D. Smith, J.R. Gardinier, Eur. J. Inorg. Chem. (2008) 3200–3211.
[48] Z.R. Grabowski, K. Rotkiewicz, W. Rettig, Chem. Rev. 103 (2003) 3899–4031.
[49] L.G.S. Brooker, F.L. White, R.H. Sprague, S.G. Dent, G. Van Zandt, Chem. Rev. 41 (1947) 325–351.
[50] H.C. Longuet-Higgins, J. Chem. Phys. 18 (1950) 265–274.
[51] D. Huang, Y. Chen, J. Zhao, Dyes Pigm. 95 (2012) 732–742.
[52] G.J. Huang, J.H. Ho, C. Prabhakar, Y.H. Liu, S.M. Peng, J.S. Yang, Org. Lett. 14 (2012) 5034–5037.
[53] B. Wang, H. Liao, H. Yeh, W. Wu, C. Chen, J. Lumin. 113 (2005) 321–328.
[54] C. Cornelissen-Gude, W. Rettig, J. Phys. Chem. A 103 (1999) 4371–4377.
[55] G. Ulrich, R. Ziessel, A. Harriman, Angew. Chem. Int. Ed. 46 (2007) 2–20.
[56] J.-Q. Feng, B.-L. Liang, D.-L. Wang, L. Xue, X.-Y. Li, Org. Lett. 10 (2008) 4437–4440.
[57] P.E. Burrows, Z. Shen, V. Bulovic, D.M. McCarty, S.R. Forrest, J.A. Cronin, M.E. Thompson, J. Appl. Phys. 79 (1996) 7991–8006.
[58] N.J. Turro, Modern Molecular Photochemistry, University Science Books, Mill Valley, 1991.
[59] J. Schäer, M. Scheurer, B. Speiser, W. Kuźnik, I.V. Kityk, Spectrochim. Acta A: Mol. Biomol. Spectro. 95 (2012) 193–198.
[60] J.-M. Zhao, H.-Y. Lu, J. Cao, Y. Jiang, C.-F. Chen, Tetrahedron Lett. 50 (2009) 219–222.
[61] Q.T. Miao, H.Q. Sun, J. East China Inst. Chem. Technol. 18 (1992) 765–771.
[62] K. Krumova, G. Cosa, J. Am. Chem. Soc. 132 (2010) 17560–17569.
[63] T. Wang, Y. Chen, X. Bao, Z. Du, J. Guo, N. Wang, M. Sun, R. Yang, Dyes Pigm. 98 (2013) 11–16.
[64] J.-C. Chen, C.-J. Chiang, Y.C. Liu, Synth. Met. 160 (2010) 1953–1961.
[65] V.V. Pavlishchuk, A.W. Addison, Inorg. Chim. Acta 298 (2000) 97–102.